International Journal of Microwave and Wireless Technologies

cambridge.org/mrf

Research Paper

Cite this article: Yang Y, Qi Z, Chen Y, Li X (2024) Multi-band circularly polarized antenna for WLAN and WiMAX applications based on characteristic mode theory. *International Journal of Microwave and Wireless Technologies* **16**(6), 1071–1079. https://doi.org/10.1017/S1759078724000114

Received: 29 August 2023
Revised: 23 December 2023
Accepted: 5 January 2024

Keywords:
broadband; characteristic mode theory; circular polarization; multi-band antenna

Corresponding author: Zihang Qi;
Email: qizihang@bupt.edu.cn

Multi-band circularly polarized antenna for WLAN and WiMAX applications based on characteristic mode theory

Yutong Yang, Zihang Qi, Yongxin Chen and Xiuping Li

State Key Laboratory of Information Photonics and Optical Communications, The Key Laboratory of Universal Wireless Communications of Ministry of Education, Beijing Key Laboratory of Work Safety Intelligent Monitoring, The School of Electronic Engineering, Beijing University of Posts and Telecommunications, Beijing, China

Abstract

A multi-band circularly polarized antenna is proposed for WLAN (2.4/5.3/5.8 GHz) and WiMAX (3.5 GHz) applications. The proposed antenna is constructed of a radiation patch and a reflecting metal ground. Characteristic mode theory is utilized to analyze the modes of the patch and based on these results the antenna is optimized. The −10 dB impedance bandwidths of the proposed antenna are 53.53% (2.4–4.15 GHz) and 47.28% (5.25–8.5 GHz), respectively. The antenna radiates left-handed circular polarization in the lower band and right-handed circular polarization in the upper band. A maximum gain of 10 dBic is achieved for the proposed antenna.

Introduction

Circularly polarized antennas can accept arbitrary polarization of the coming wave and have a wide range of applications in wireless communications [1], such as global positioning system (GPS), radio frequency identification (RFID), satellite communications, wireless local area networks (WLAN), etc. Multi-band operation has become a hot topic in the current research of the new electronic devices, which can work flexibly in multiple communication states. Therefore, various types of multi-band antennas have emerged and how to achieve better communication applications is a popular research question in current multi-band antenna design [2–7].

Various types of multi-band antennas have been designed in wireless communication systems. Sharma et al. [8] presented a quad-band circularly polarized dielectric resonator antenna for GPS/CNSS/WLAN/WiMAX applications. In [9], a crossed dipole on a high impedance surface was proposed for triple-band WLAN applications. Slot antennas are more often chosen in multi-band antenna design. However, slot antennas are more complicated to implement, such as comb slot [10], multi-branch slot [5], non-concentric circles slot and so on. The multi-band patch antenna is another option for researchers [11–14].

Characteristic mode theory (CMT) was first proposed by Garbacz and Turpin as a set of modes diagonalizing a scattering matrix in 1965 [15] and refined by Harrington and Mautz for perfectly electrically conducting (PEC) object in 1971 [16, 17] that the current distribution can be considered as a linear superposition of the modal currents. CMT was developed in dielectric and magnetic bodies [18, 19], and then generalized for antenna design [20].

The patch antennas are designed for a wide range of applications using characteristic mode analysis (CMA), such as multi-mode MIMO antenna [21] and orbital angular momentum (OAM) [22]. The circular polarization patch antennas are achieved by making two characteristic modes orthogonal and the character angle difference is 90° and the broadband characteristic is realized by the resonate frequency points of multiple modes [23–26]. In [27], the multi-band characteristics were achieved by five modes separations, but only two bands were obtained. Therefore, using CMA to design multi-band patch antennas is worth studying.

This paper presents a multi-band circularly polarized patch antenna for WLAN and WiMAX applications based on the characteristic mode theory. In section "Multi-band circularly polarized antenna," the antenna design process is completed in the order of characteristic mode analysis, feed design, and the influence of important geometric parameters. The simulated and measured results of the antenna are presented and discussed in section "Results of simulation and measurement," and the full-wave simulation and measured results verify the CMT. Conclusion is presented in last section.

Multi-band circularly polarized antenna

Characteristic mode theory

The total current J on the antenna surface can be written as the superposition of multiple characteristic modal currents as (1) according to CMT [15]:

$$J = \sum_{1}^{N} \alpha_n J_n, \tag{1}$$

where J_n is the nth characteristic current and α_n is a complex modal weighting coefficient (MWC), which can be written as (2):

$$MWC = \alpha_n = \frac{\langle J_n, E^i \rangle}{(1 + j\lambda_n)}, \tag{2}$$

λ_n is the real eigenvalue solved by the eigenvalue equation and E^i is the incident electric field [28].

MS in (3) is the modal significance, defined as the normalized current amplitude. MS is an inherent property of the mode and is independent of the external source. Characteristic angle (CA) is another important parameter, defined as shown in (4). CA characterizes the phase difference between the characteristic current J_n and the associated electric field E_n. The mode is considered significant when MS is close to 1 or CA is close to 180°:

$$MS_n = \left| \frac{1}{1 + j\lambda_n} \right|, \tag{3}$$

$$CA_n = 180^\circ - \tan^{-1} \lambda_n. \tag{4}$$

The modes used to achieve the circular polarization should satisfy the following conditions:

(1) **MS**
The MS curves of the two modes intersect means that the MS values are equal.
(2) **CA**
CA difference between the two modes is around 90°.
(3) **Characteristic Current**
The current of the two modes should be excited simultaneously and the direction should be perpendicular.
(4) **Directivity**
The directivity of the two modal radiation patterns is consistent.

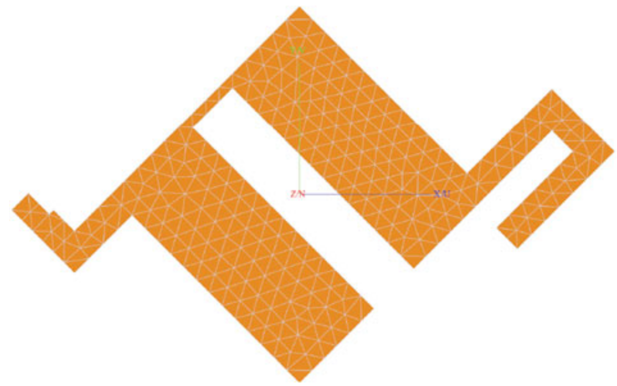

Figure 1. Antenna structure without feeding network and metal ground in FEKO.

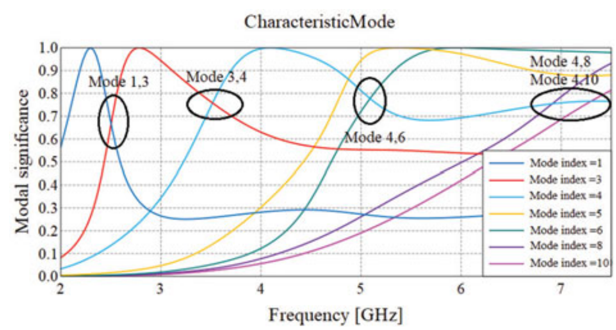

Figure 2. Modal significance curves without feeding structure.

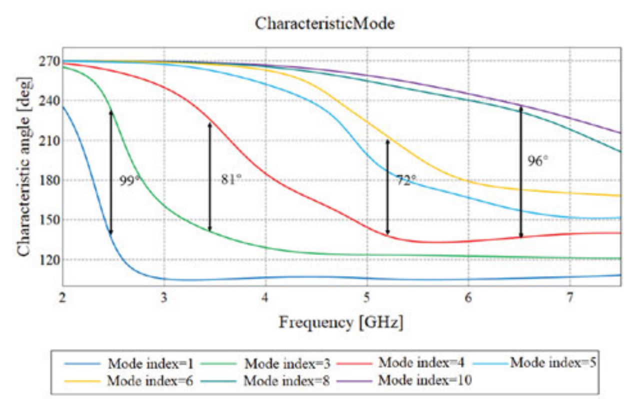

Figure 3. CA curves without feeding structure.

CMA of the multi-band antenna without excitation

Although the characteristic mode analysis of antennas with substrate has been studied [18], the influence of substrate on the mode of the proposed antenna is limited. In this section, FEKO is utilized to do the CMA of the radiating patch in Fig. 1, which is derived from a combination of multiple rectangles. The first 15 modes of the radiating patch without feeding structure are computed. The final structure is obtained by optimizing the parameters of the antenna with substrate. Figure 2 shows the MS curves, it can be seen that a small number of modes and simple distribution in the low frequency band and a large number of modes and complex distribution in the high frequency band. It is worth noting that the significance curves of different modes have intersection points, such as modes 1 and 3 intersects at 2.5 GHz, modes 3 and 4 intersects at 4.5 GHz, modes 4 and 6 intersects at 5.3 GHz and so on. According to the CMT, modes are called significant modes when MS *gt* 0.707, so the main significant modes around 7 GHz are modes 4, 8, and 10.

Besides, the circular polarization also requires attention to the difference of the CA between two orthogonal modes with the same current amplitude. As shown in Fig. 3, the CA phase difference of the intersecting modes are 99°, 81°, 78°, and 96° at 2.5, 3.5, 5.3, and 6.5 GHz where the MS curves intersect, respectively. It can be observed that the CA curves change slowly around 6.5 GHz, which indicates that there is potential to form a broadband circular polarization.

The characteristic currents and the radiation patterns of each mode at the corresponding frequencies are shown in Figs. 4 and 5. Fig. 4(a, b) shows the current distribution of modes 1 and 3 at

https://doi.org/10.1017/S1759078724000114 Published online by Cambridge University Press

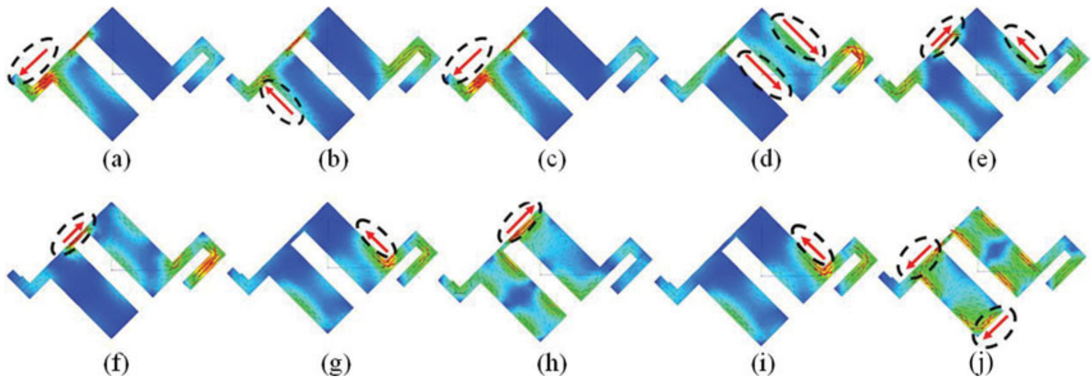

Figure 4. Characteristic currents of the antenna without feeding structure: (a) mode 1 at 2.5 GHz, (b) mode 3 at 2.5 GHz, (c) mode 3 at 3.5 GHz, (d) mode 4 at 3.5 GHz, (e) mode 4 at 5.3 GHz, (f) mode 6 at 5.3 GHz, (g) mode 4 at 6.5 GHz, (h) mode 8 at 6.5 GHz, (i) mode 4 at 6.5 GHz, and (j) mode 10 at 6.5 GHz.

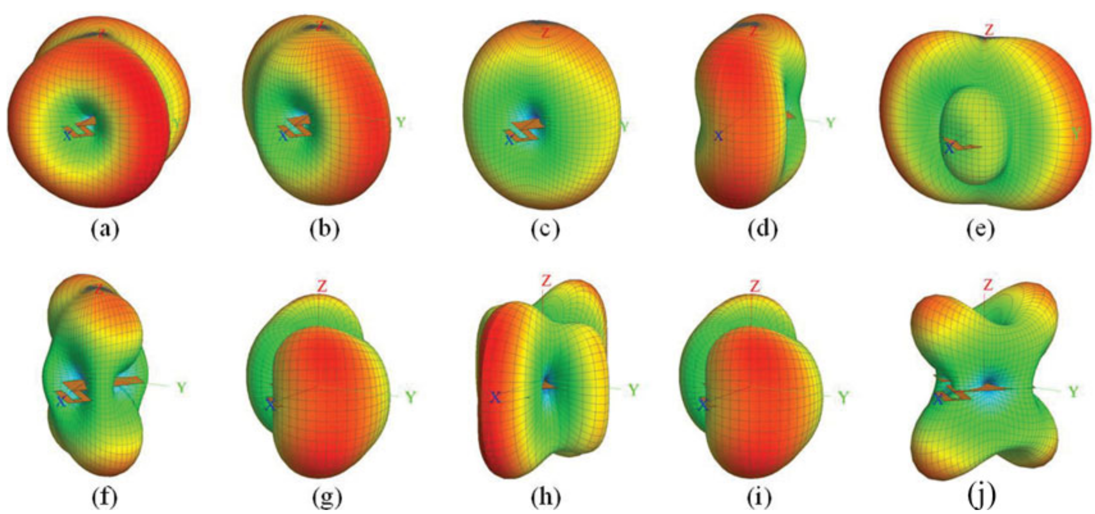

Figure 5. Radiation patterns of the antenna without feeding structure: (a) mode 1 at 2.5 GHz, (b) mode 3 at 2.5 GHz, (c) mode 3 at 3.5 GHz, (d) mode 4 at 3.5 GHz, (e) mode 4 at 5.3 GHz, (f) mode 6 at 5.3 GHz, (g) mode 4 at 6.5 GHz, (h) mode 8 at 6.5 GHz, (i) mode 4 at 6.5 GHz, and (j) mode 10 at 6.5 GHz.

2.5 GHz, both with vertical directions, and in turn (c, d) show the current distribution of modes 3 and 4 at 3.5 GHz, (e, f) show the current distribution of modes 4 and 6 at 5.3 GHz, (g, h) show the current distribution of mode 4 and mode 8 at 6.5 GHz, (i, j) show the current distribution of mode 4 and mode 10 at 6.5 GHz. As shown in Fig. 5,the radiation direction of each orthogonal modes at 3.5, 5.3, and 6.5 GHz is consistent.

It is known that the two orthogonal modes have equal MS. When their CA difference is around 90°, circular polarization can be achieved. All of the characteristic modes have orthogonal current direction and the consistent radiation directivity at the same frequency, respectively. The above performances meet the four conditions for circular polarization under the CMA, so the antenna structure can theoretically achieve multi-band circular polarization performance.

CMA of the multi-band antenna with feeding structure

The configuration of the proposed antenna is built in the full wave simulation software HFSS as shown in Fig. 6. Rogers 5880 is chosen as the dielectric substrate with a thickness of 1.575 mm and a relative permittivity of 2.2. The upper layer of the substrate is the radiating part of the antenna, and the apex of the largest square of the radiating part is used as the feeding position. Microstrip structure is used for antenna feeding and the microstrip transition is used to adjust the impedance matching. A metal ground is placed at 33.5 mm below the antenna as a reflector. The design of antennas with substrate will have a certain impact on the characteristic mode analysis [20], so the optimized geometric parameters are shown in Fig. 6.

Whether the characteristic mode can be excited as desired depends on the selection of the feeding position. In Fig. 7, four points are selected on the radiation structure for performance comparison through microstrip feeding. From the performance of impedance matching and axial ratio in Figs. 8 and 9, feeding-1 can excite all the modes in second section), in which the impedance bandwidth covers 2.45, 3.5, 5.8, and 6.5 GHz, and the resonance frequencies of AR are at 2.45, 3.5, 5.3, 5.8, and 6.6 GHz. While the impedance bandwidth of the other three feeding points cannot cover all the desired frequency bands. Therefore, the feeding-1 point is selected as the feeding position.

Figures 10 and 11 show the characteristic currents and the radiation patterns of the radiation part when feeding at the feeding-1 position, in which characteristic modes have vertical current

https://doi.org/10.1017/S1759078724000114 Published online by Cambridge University Press

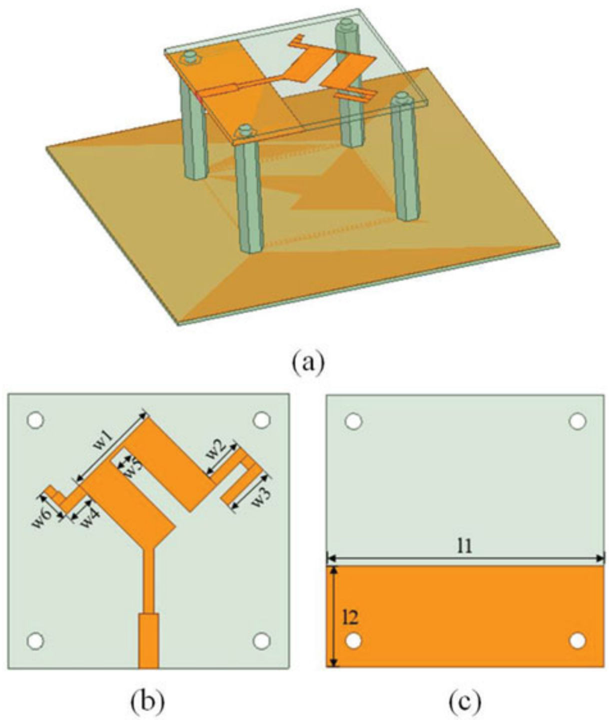

Figure 6. Configuration of the structure.(a) Antenna, (b) top view, (c) bottom view. $w1 = 18$ mm, $w2 = 8.1$ mm, $w3 = 9.3$ mm, $w4 = 5.4$ mm, $w5 = 3.8$ mm, $w6 = 6$ mm, $l1 = 52$ mm, $l2 = 19$ mm.

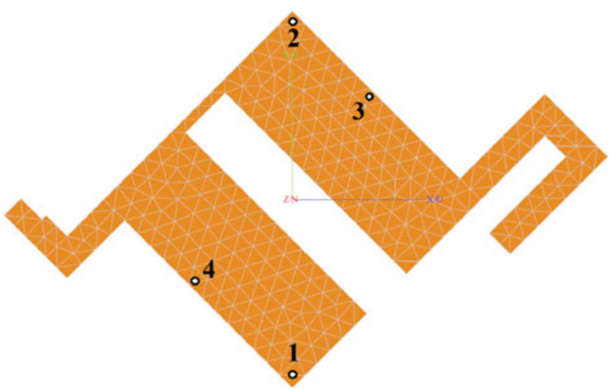

Figure 7. Configuration of the structure for feeding position.

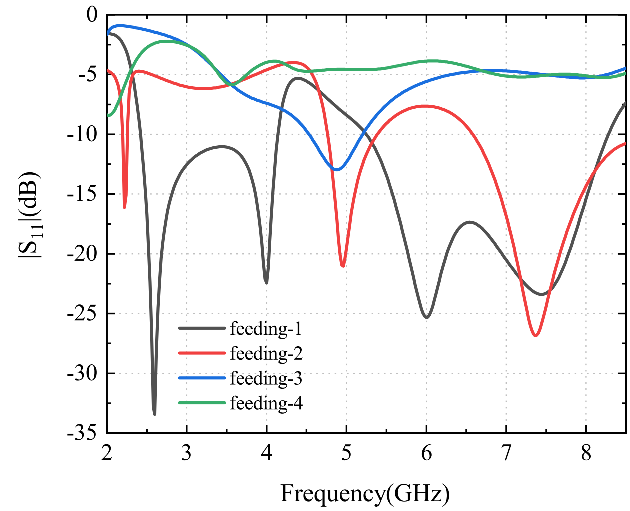

Figure 8. The S-parameter for different feeding positions.

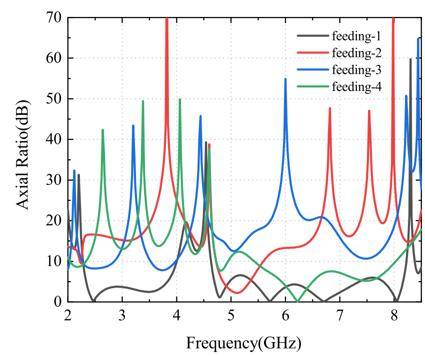

Figure 9. The AR for different feeding positions.

direction and the consistent radiation directivity at the resonant frequency. Figures 12 and 13 show the MS and CA curves, in which the feeding structure has a significant impact on modes 5 and 8, and the MS curve intersection frequency point of modes 4 and 6 has moved from 5.3 to 4.9 GHz, but the circular polarization performance is basically not affected, so that satisfying the circular polarization condition. The changes in CMA before and after adding the feed structure are shown in Table 1.

Effect of antenna geometric parameters

The effect of the geometric parameters on antenna performance is introduced in more detail in this section. Figure 14(a) shows the effect of the width *l2* of the bottom metal slab at radiation layer on $|S_{11}|$. Notably, as *l2* increases, the impedance matching at low band shifts to better, but first widens and then deteriorates at high band. So *l2* of 19 mm is the most suitable, which not only reduces the downward radiation of the microstrip feeding line, but also reduces the influence on the field distribution and impedance of the radiation structure. In Fig. 14(b), the AR is mainly affected by *w5* at low band. As *w5* increases, the curve at 2.5 GHz shifts to low frequency, and the bandwidth at 3.5 GHz increases. In Fig. 14(c), *w3* has the opposite effect on the axial ratio at 6 and 7.5 GHz. So compromise $w5 = 3.8$ mm, $w3 = 9.3$ mm.

h is an important value because it satisfies the reflections of multiple bands. Due to the higher frequency, the shorter the wavelength, making it more sensitive to the effect on high band. From Fig. 14(d)–(f), it can be seen that a decrease in *h* is beneficial for improving the performance of axial ratio and cross polarization level. However, considering the possible machining errors, $|S_{11}|$ may be higher than −10 dB at 3.5 GHz, so $h = 33.5$ mm is chosen.

Results of simulation and measurement

In order to verify the proposed multi-band circularly polarized performance, the antenna is fabricated and measured as shown in Fig. 15. Figure 16 shows the S-parameter simulated and measured results of the multi-band circularly polarized antenna. From the simulation results, it can be seen that there are two resonance points around 2.6 and 4 GHz, which are known from second section to be the series resonance points caused by modes 1 and 4, respectively. It is known from the CMA that the number of

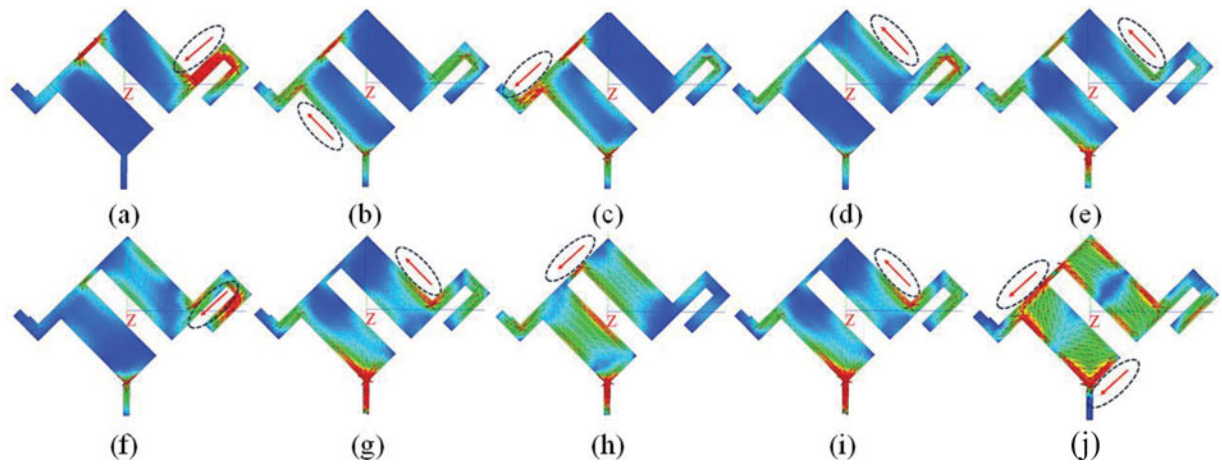

Figure 10. Characteristic currents of the antenna with feeding structure: (a) mode 1 at 2.5 GHz, (b) mode 3 at 2.5 GHz, (c) mode 3 at 3.5 GHz, (d) mode 4 at 3.5 GHz, (e) mode 4 at 4.9 GHz, (f) mode 6 at 4.9 GHz, (g) mode 4 at 5.8 GHz, (h) mode 8 at 5.8 GHz, (i) mode 4 at 6.5 GHz, and (j) mode 10 at 6.5 GHz.

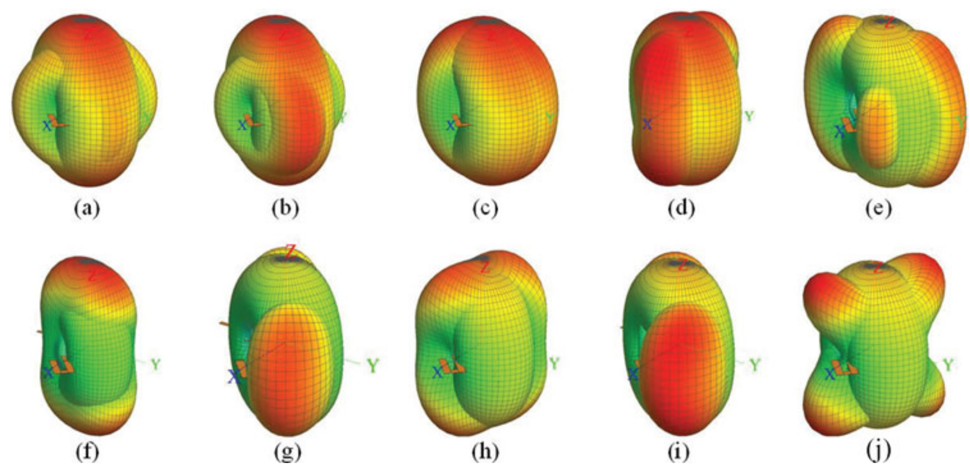

Figure 11. Radiation patterns of the antenna with feeding structure: (a) mode 1 at 2.5 GHz, (b) mode 3 at 2.5 GHz, (c) mode 3 at 3.5 GHz, (d) mode 4 at 3.5 GHz, (e) mode 4 at 4.9 GHz, (f) mode 6 at 1.9 GHz, (g) mode 4 at 5.8 GHz, (h) mode 8 at 5.8 GHz, (i) mode 4 at 6.5 GHz, and (j) mode 10 at 6.5 GHz.

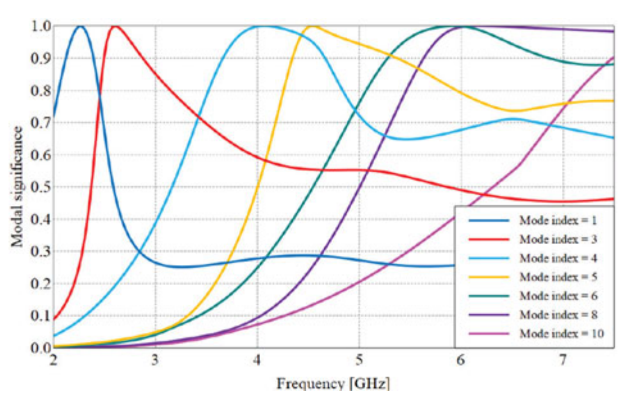

Figure 12. Modal significance curves with feeding structure.

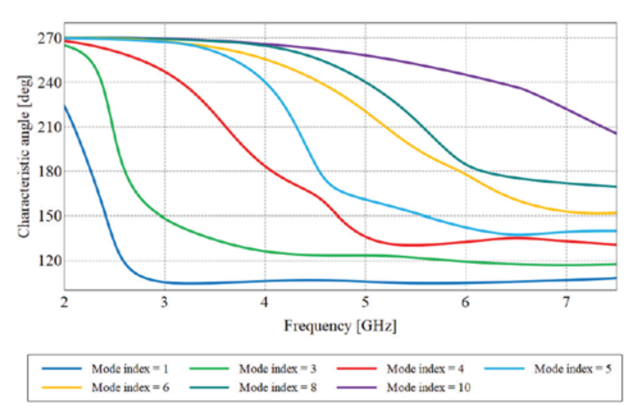

Figure 13. CA curves with feeding structure.

resonant modes increase around 6.5 GHz, so that all impedance matching is achieved above 5.2 GHz. The simulated impedance bandwidth ($|S_{11}| \leq -10$ dB) is 53.53% and 47.28% (2.4–4.15, 5.25–8.5 GHz). The measured impedance bandwidth is 52.43% and 42.8% (2.43–4.2, 5.5–8.5 GHz). The minor discrimination between the simulation and measurement may be due to the assembly and fabrication tolerance.

Axis ratio (AR) is an important parameter for circularly polarized antennas, which directly reflects the purity of circular polarization. Figure 17 shows simulated results of the AR of

Table 1. Comparison between with and without feeding structure in CMA

CMA without feeding	CMA with feeding
2.4 GHz	2.4 GHz
3.5 GHz	3.5 GHz
5.3 GHz	4.9 GHz
5.8 GHz	5.3 GHz
6.7–7 GHz	5.8–7 GHz

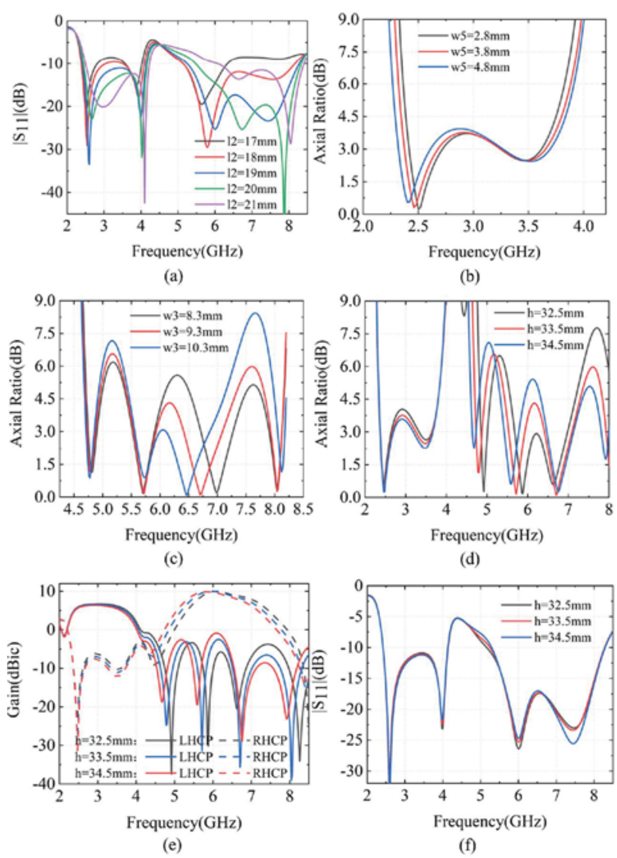

Figure 14. Effect of parameters on performance. (a) The effect of l2 on S-parameter. (b) The effect of w5 on AR. (c) The effect of w3 on AR. (d) The effect of h on AR. (e) The effect of h on gain. (f) The effect of h on S-parameter.

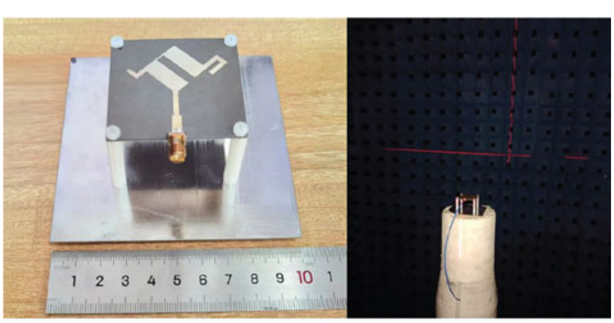

Figure 15. Photograph of fabricated antenna and measurement setup.

the multi-band antenna, which is less than 3 dB in the bands of 2.38–2.7, 3.2–3.7, 4.6–4.8, and 6.38–7.02 GHz. The wider AR at 6.5 GHz also confirms the conclusion of the CMA that a constant and

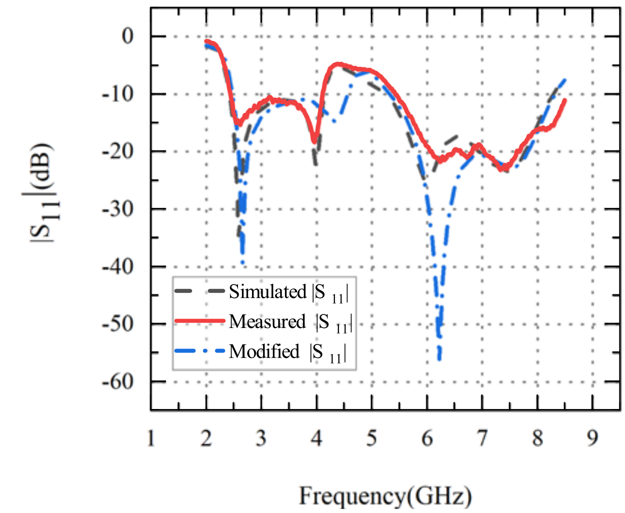

Figure 16. The S-parameter of the antenna.

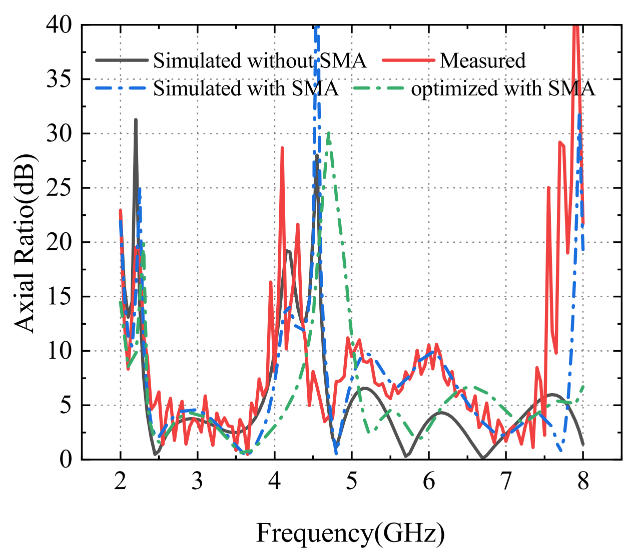

Figure 17. The axis ratio of the antenna.

Table 2. Comparison between the results of characteristic mode analysis and full wave simulations

Full-wave simulation	CMA
2.38–2.69 GHz	2.4 GHz
3.21–3.67 GHz	3.5 GHz
4.68–4.8 GHz	4.9 GHz
5.49–5.87 GHz	5.8 GHz
6.38–7.02 GHz	6.7–7 GHz

stable CA difference in this band will provide a broad AR bandwidth. The above bandwidths are in general agreement with the results of the CMA at 2.4, 3.5, 5.8, and 6.7 GHz. Due to the MS curve after adding the feeding structure shifted from 5.3 GHz to around 4.9 GHz, which is slightly different from the initial expected results. Table 2 shows the comparison between the results of full wave simulation and CMA with the feeding structure. It can be seen that the antenna operating frequency is basically the same.

https://doi.org/10.1017/S1759078724000114 Published online by Cambridge University Press

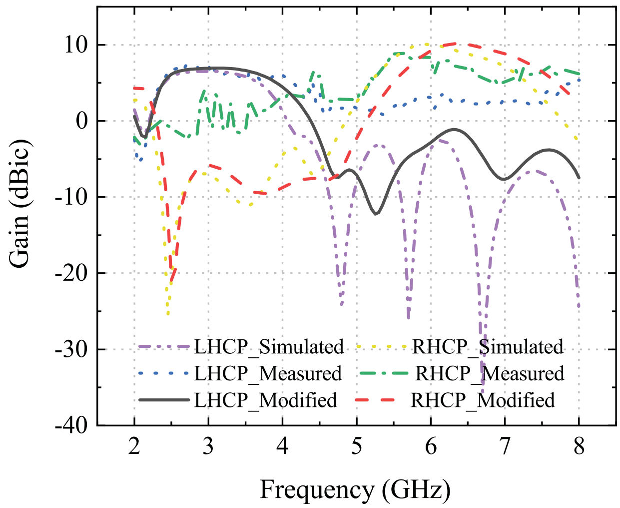

Figure 18. The gain of the antenna.

The gain of the multi-band circularly polarized antenna is shown in Fig. 18 with left-hand circular polarization at 2.5 and 3.5 GHz, and right-hand circular polarization at 5.8 and 6.5 GHz. The maximum gain of the antenna can reach 6.42 and 10.0 dBic respectively. From the conclusions of the CMA in second section, there are multiple pairs of orthogonal modes around 6.5 GHz, which are linearly superimposed on the right-hand circularly polarized mode, resulting in a significant gain increase. The simulated and measured radiation patterns in 0° and 90° planes at 2.45, 3.5, 5.3, and 5.8 GHz are shown in Fig. 19. The measured results match well with the simulated results at the frequency bands.

In Fig. 17, the measured results do not have good consistency with the simulated results, which is due to the use of the ideal lumped port for feeding in the simulation without considering the influence of the SMA connector. After the measured results are generated, an antenna structure with a SMA connector is simulated again. It can be seen that the AR curve with a SMA connector is mostly consistent with the test results, thus verifying the above conjecture. Finally, an antenna structure with SMA connector is optimized also shown in Figs. 16, 17, and 18. The modified impedance bandwidth ($|S_{11}| \leq -10$ dB) is 60.03% and 44.35% (2.46–4.57, 5.3–8.32 GHz). The 3 dB axis ratio bandwidth covers 2.4–2.65, 3.25–4, 5.18–5.35, and 5.7–6.05 GHz, respectively. The maximum gain reaches 6.5 and 10 dBic at LHCP and RHCP, respectively.

Table 3 shows the performance comparison of several multi-band antennas. Compared to [29] and [30], the proposed antenna has similar dimensions but significant advantages in terms of gain. Although it has good multi frequency performance in [31] and [10], it does not cover frequency bands above 5 GHz, and there is no advantage in $|S_{11}|$ bandwidth. Overall, the proposed antenna can utilize the characteristic mode theory and highlight the advantages of high gain and multiple bands in a single radiation patch design.

Conclusion

This paper proposed a multi-band circularly polarized antenna for WLAN and WiMAX applications based on characteristic mode theory. The antenna can support 2.4, 5.8, 6.4–7 GHz WLAN bands and 3.5 GHz, 5.3 GHz WiMAX bands simultaneously. The antenna provides sufficient bandwidth in the communication band with a high gain of 10 dBic around 6.5 GHz. The antenna possesses advantages of compact size, simple feed structure and low cost as compared to other similar antennas, making it an excellent candidate for sub-6 GHz communication applications.

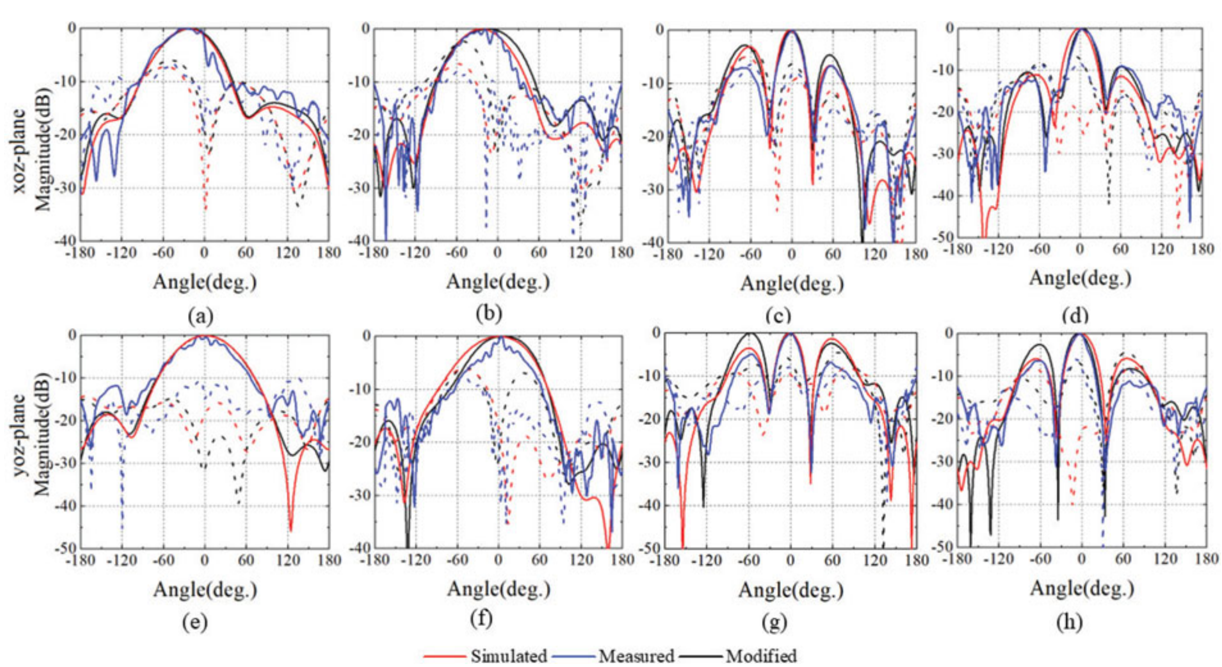

Figure 19. The simulated and measured radiation patterns of the proposed antenna. Xoz-plane: (a) 2.45 GHz, (b) 3.5 GHz, (c) 5.3 GHz, (d) 5.8 GHz; Yoz-plane: (e) 2.45 GHz, (f) 3.5 GHz, (g) 5.3 GHz, and (h) 5.8 GHz.

https://doi.org/10.1017/S1759078724000114 Published online by Cambridge University Press

Table 3. Comparison of the performance with other similar antennas

References	Impedance bandwidth	AR bandwidth	Maximum of Gain (dBic)	Size (mm^3)
[29]	2.56 GHz: 14.8% 5.7 GHz: 80.7%	2.575 GHz: 5.4% 3.6 GHz: 8.3% 5.35 GHz: 3.7% 5.785 GHz: 2.9%	5.95 6.92 6.37 6.07	52*55*32.5
[30]	1.83 GHz: 21.4% 2.5 GHz: 12.8% 3.1 GHz: 4.5%	4.37% 11.9% 3.6%	2.7 4.2 3.5	50*50*1.56
[31]	1.085 GHz: 21.1% 1.56 GHz: 12.8% 2.18 GHz: 27.1% 2.65 GHz: 7.54%	11.65% 7.64% 7.01% 7.1%	NG	120*120*28
[10]	0.7–0.73 GHz: 4.2% 1.16-1.2 GHz: 3.39% 1.3–1.32 GHz: 1.53% 1.57–1.62 GHz: 3.13% 2.3–2.5 GHz: 8.33% 2.7–3.5 GHz: 25.81%	1.16–1.19 GHz: 2.55% 1.56–1.58 GHz: 1.27% 3.1–3.2 GHz: 3.17% 3.48–3.5 GHz: 0.57%	4.6 4.5 6.8 4.3 6.3 9	150*100*19.2
This paper	2.4–4.15 GHz: 53.53% 5.25–8.5 GHz: 47.28%	2.38–2.69 GHz: 11.8% 3.21–3.67 GHz: 13.4% 5.49–5.87 GHz: 6.7% 6.38–7.02 GHz: 9.6%	6.3 6.42 10.0 9.2	51*51*33.5

NG: not given.

Acknowledgements. This work was supported by National Key R&D Program of China (No. 2022YFF0604200).

Competing interests. None declared.

References

1. **Gao S, Luo Q and Zhu F** (2013) *Circularly Polarized Antennas*. New York: Wiley-IEEE Press.
2. **Verma S and Kumar P** (2014) Compact triple-band antenna for WiMAX and WLAN applications. *Electronics Letters* **50**, 484–486.
3. **Wu T, Shi XW, Li P and Bai H** (2013) Tri-band microstrip-fed monopole antenna with dual-polarisation characteristics for WLAN and WiMAX applications. *Electronics Letters* **49**, 1597–1598.
4. **Le TT and Park HC** (2014) Very simple circularly polarised printed patch antenna with enhanced bandwidth. *Electronics Letters* **50**, 1896–1898.
5. **Baek JG and Hwang KC** (2013) Triple-band unidirectional circularly polarized hexagonal slot antenna with multiple L-shaped slits. *IEEE Transactions on Antennas and Propagation* **61**, 4831–4835.
6. **Bao XL and Ammann MJ** (2014) Printed triple-band circularly polarised antenna for wireless systems. *Electronics Letters* **50**, 1664–1665.
7. **Hoang TV and Park HC** (2014) Very simple 2.45/3.5/5.8 GHz triple-band circularly polarised printed monopole antenna with bandwidth enhancement. *Electronics Letters* **50**, 1792–1793.
8. **Sharma A, Das G, Gupta S and Gangwar RK** (2020) Quad-band quad-sense circularly polarized dielectric resonator antenna for GPS/CNSS/WLAN/WiMAX applications. *IEEE Antennas and Wireless Propagation Letters* **19**, 403–407.
9. **Ta SX, Park I and Ziolkowski RW** (2013) Circularly polarized crossed dipole on an HIS for 2.4/5.2/5.8-GHz WLAN applications. *IEEE Antennas and Wireless Propagation Letters* **12**, 1464–1467.
10. **Abdalrazik A, Gomaa A and Kishk** (2021) A hexaband quad-circular-polarization slotted patch antenna for 5G, GPS, WLAN, LTE, and radio navigation applications. *IEEE Antennas and Wireless Propagation Letters* **20**, 1438–1442.
11. **Lu JH and Huang BJ** (2013) Planar compact slot antenna with multi-band operation for IEEE 802.16m application. *IEEE Transactions on Antennas and Propagation* **61**, 1411–1414.
12. **Deshmukh AA and Ray KP** (2010) Multi-band configurations of stub-loaded slotted rectangular microstrip antennas. *IEEE Antennas and Propagation Magazine* **52**, 89–103.
13. **Luo Y, Zhu L, Liu Y, Liu NW and Gong S** (2022) Multiband monopole smartphone antenna with bandwidth enhancement under radiation of multiple same-order modes. *IEEE Transactions on Antennas and Propagation* **70**, 2580–2592.
14. **Qian JF, Chen FC, Xiang KR and Chu QX** (2019) Resonator-loaded multi-band microstrip slot antennas with bidirectional radiation patterns. *IEEE Transactions on Antennas and Propagation* **67**, 6661–6666.
15. **Garbacz RJ** (1965) Modal expansions for resonance scattering phenomena. *Proceedings of the IEEE* **53**, 856–864.
16. **Harrington R, Mautz J and Chang Y** (1972) Characteristic modes for dielectric and magnetic bodies. *IEEE Transactions on Antennas and Propagation* **20**, 194–198.
17. **Chang Y and Harrington R** (1977) A surface formulation for characteristic modes of material bodies. *IEEE Transactions on Antennas and Propagation* **25**, 789–795.
18. **Chen YK and Wang CF** (2015) *Characteristic Modes: Theory and Applications in Antenna Engineering*. Hoboken, NJ: Wiley Publishing.
19. **Harrington R and Mautz J** (1971) Theory of characteristic modes for conducting bodies. *IEEE Transactions on Antennas and Propagation* **19**, 622–628.
20. **Harrington R and Mautz J** (1971) Computation of characteristic modes for conducting bodies. *IEEE Transactions on Antennas and Propagation* **19**, 629–639.
21. **Sharma A, Das G, Gupta S and Gangwar** (2020) Quad-band quad-sense circularly polarized dielectric resonator antenna for GPS/CNSS/WLAN/WiMAX applications. *IEEE Antennas and Wireless Propagation Letters* **19**, 403–407.
22. **Parvin M, Ahmadi-Shokouh J and Dashti H** (2020) Systematic feed locating in multi-mode MIMO antennas using characteristic mode theory. *AEU – International Journal of Electronics and Communications* **126**, 1434–8411.
23. **Li Q, Li W, Zhu J, Zhang L and Liu Y** (2020) Implementing orbital angular momentum modes using single-fed rectangular patch antenna. *International Journal of RF and Microwave Computer-Aided Engineering* **30**, 5.
24. **Tao S Xu M, Ding Z, Wu Z, Wang H and Wang Y** (2022) A wideband circularly polarized monopole antenna with elliptic ring slot patch using

characteristic mode analysis. *International Journal of RF and Microwave Computer-Aided Engineering* **32**, 12.
25. **Sharma A** (2021) Design of compact wideband circularly polarized hexagon-shaped antenna using characteristics mode analysis. *IEEE Transactions on Antennas and Propagation* **70**, 1–8.
26. **Zeng J, Zhang Z, Lin FH and Guan F** (2022) Penta-mode ultrawideband circularly polarized stacked patch antennas using characteristic mode analysis. *IEEE Transactions on Antennas and Propagation* **70**, 9051–9060.
27. **Xu W, Nan J, Liu J and Agostino FD** (2022) Broadband circularly polarized antennas with compact radiator using characteristic mode analysis. *International Journal of Antennas and Propagation* **99**, 1–13.
28. **Deng H** (2022) Design of multimode broadband circularly polarized antenna using characteristics mode analysis. *International Journal of RF and Microwave Computer-Aided Engineering* **32**, 12.
29. **Garbacz RJ and Turpin R** (1971) A generalized expansion for radiated and scattered fields. *IEEE Transactions on Antennas and Propagation* **19**, 348–358.
30. **Hoang TV, Le TT, Li QY and Park HC** (2016) Quad-band circularly polarized antenna for 2.4/5.3/5.8-GHz WLAN and 3.5-GHz WiMAX applications. *IEEE Antennas and Wireless Propagation Letters* **15**, 1032–1035.
31. **Paul PM, Kandasamy K and Sharawi MS** (2018) A triband circularly polarized strip and SRR-loaded slot antenna. *IEEE Transactions on Antennas and Propagation* **66**, 5569–5573.

Yutong Yang received the B.E. degree in electronic information science and technology from Xidian University, Xian, China, in 2021. She is currently pursuing the M.S. degree in electronic science and technology from Beijing University of Posts and Telecommunications. Her current research interests include characteristic modes theory and millimeter-wave antennas.

Zihang Qi received the B.E. degree in electronic and information engineering from China Three Gorges University, Yichang, China, in 2013, and the Ph.D. degree in electronic science and technology from the Beijing University of Posts and Telecommunications, Beijing, China, in 2019. He is currently an associate research fellow with the Beijing University of Posts and Telecommunications. His current research interests include OAM antennas, millimeter-wave/THz antennas and microwave filters.

Yongxin Chen received the B.S. degree in Electronic Information Science and Technology from Nanjing University of Aeronautics and Astronautics, Nanjing, China. And, the M.S. degree in electronic engineering from Beijing University of Posts and Telecommunications, Beijing, China. His current research interests includecharacteristic modes theory.

Xiuping Li received the B.S. degree from Shandong University in 1996, the Ph.D. degree from Beijing Institute of Technology in 2001.From 2001 to 2003, she joined in Positioning and Wireless Technology Center, Nanyang Technological University, where she was a research fellow and involved in the research and development of RFID system. In 2003, she was a research professor in Yonsei University, South Korea. Since 2004, she joined Beijing University of Posts and Telecommunications as associate professor, and promoted to professor in 2009. She has been selected into the New Century Excellent Talents Support Plan in National Ministry of Education, the Beijing Science and Technology Nova Support Plan. She won the second prize of the Progress in Science and Technology of China Institute of Communications and the Excellent Achievements in Scientific Research of Colleges and Universities. Her research interests include millimeter-wave antennas, THz antennas, RFID systems, and MMIC design.

https://doi.org/10.1017/S1759078724000114 Published online by Cambridge University Press